

## Theoretical models for electrochemical impedance spectroscopy and local $\zeta$ -potential of unfolded proteins in nanopores

Michael J. Vitarelli and David S. Talaga

Citation: *J. Chem. Phys.* **139**, 105101 (2013); doi: 10.1063/1.4819470

View online: <http://dx.doi.org/10.1063/1.4819470>

View Table of Contents: <http://jcp.aip.org/resource/1/JCPSA6/v139/i10>

Published by the AIP Publishing LLC.

---

### Additional information on *J. Chem. Phys.*

Journal Homepage: <http://jcp.aip.org/>

Journal Information: [http://jcp.aip.org/about/about\\_the\\_journal](http://jcp.aip.org/about/about_the_journal)

Top downloads: [http://jcp.aip.org/features/most\\_downloaded](http://jcp.aip.org/features/most_downloaded)

Information for Authors: <http://jcp.aip.org/authors>



[www.goodfellowusa.com](http://www.goodfellowusa.com)

**Goodfellow**

metals • ceramics • polymers  
composites • compounds • glasses

**Save 5% • Buy online**  
70,000 products • Fast shipping

# Theoretical models for electrochemical impedance spectroscopy and local $\zeta$ -potential of unfolded proteins in nanopores

Michael J. Vitarelli, Jr.<sup>a)</sup> and David S. Talaga<sup>b)</sup>

Department of Chemistry and Biochemistry Montclair State University, 1 Normal Road, Montclair,  
New Jersey 07043, USA

(Received 6 January 2013; accepted 14 August 2013; published online 9 September 2013)

Single solid-state nanopores find increasing use for electrical detection and/or manipulation of macromolecules. These applications exploit the changes in signals due to the geometry and electrical properties of the molecular species found within the nanopore. The sensitivity and resolution of such measurements are also influenced by the geometric and electrical properties of the nanopore. This paper continues the development of an analytical theory to predict the electrochemical impedance spectra of nanopores by including the influence of the presence of an unfolded protein using the variable topology finite Warburg impedance model previously published by the authors. The local excluded volume of, and charges present on, the segment of protein sampled by the nanopore are shown to influence the shape and peak frequency of the electrochemical impedance spectrum. An analytical theory is used to relate the capacitive response of the electrical double layer at the surface of the protein to both the charge density at the protein surface and the more commonly measured zeta potential. Illustrative examples show how the theory predicts that the varying sequential regions of surface charge density and excluded volume dictated by the protein primary structure may allow for an impedance-based approach to identifying unfolded proteins. © 2013 AIP Publishing LLC. [<http://dx.doi.org/10.1063/1.4819470>]

## I. INTRODUCTION

Individually fabricated solid-state nanopores<sup>2,3</sup> have been used as synthetic systems for ion-channel studies,<sup>4–8</sup> single molecule sensing,<sup>9–11</sup> DNA resistive pulse measurements,<sup>2,11</sup> and DNA sequencing.<sup>12</sup> Resistive pulse measurements<sup>2,11</sup> apply a fixed DC potential and measure the current vs. time. Investigators typically further reduce the event data by binning the average current drop and event duration into histograms. Recently, electrochemical impedance spectroscopy (EIS),<sup>13–15</sup> which measures the impedance as a function of frequency of applied AC potential, has been used to analyze nanoporous structures.<sup>1</sup> Since the EIS signal is a measure of the electrokinetic transport of solutions through nanopores, it is sensitive to the surface properties and geometries of these nanopores.<sup>1,16,17</sup> Vitarelli *et al.*<sup>1</sup> have shown that by measuring the impedance spectrum of nanochannels in a conducting solution it is possible to obtain the nano channel geometry and the double layer specific differential capacitance at their walls. The framework of that model has sufficient flexibility to enable its extension to include the influence of large molecular species, such as proteins, within the nanopore.

This paper extends the Variable Topology finite Warburg (VTW) impedance model<sup>1</sup> to include the effect of an unfolded protein within the nanopore, see Fig. 1. The protein was modeled as a variable-radius tube with a surface-charge density that, when in a conducting solution, produces an electrical double layer specific differential capacitance along its surface.

Most proteins are globular, however proteins have been shown to unfold inside nanopores,<sup>11</sup> thus a tubular model was chosen. Most proteins have multiple charges of both signs, leading to the common occurrence that a given protein will have a point at which the charges present in the nanopore cancel creating no net force for translocation.<sup>11</sup> At these *stall points* the protein will persist in the nanopore allowing for the measurement of several EIS frequencies before the protein escapes the trap through thermal motions. For proteins that translocate too fast to resolve,<sup>11</sup> one can imagine a nanomanipulation experiment in which one end of the protein is attached to an AFM tip and slowly threaded through the nanopore. The location of the peak frequency in the imaginary component of the EIS spectrum should allow for coarse-grain resolution of sequence information through the EIS dependence on the local charge and excluded volume enabling rapid identification of single proteins by nanopores that are short compared to the protein. Note that this approach depends on the size and charge heterogeneity of polypeptide and could be extended to any polymer with similar charge and size heterogeneity. Polynucleic acids, by contrast, have very little heterogeneity in charge and size and would not be amenable to this approach.

A successful model of the impedance spectrum of an unfolded protein inside a nanopore must reproduce several physical limits. The model should show physically correct high and low frequency limits. In the low frequency limit the model should become purely resistive. The impedance of a capacitor is inversely proportional to the applied frequency, thus in the high frequency limit the model's impedance should approach zero as does an  $R \parallel C$  circuit. EIS spectra for various protein radii should show that when the radius of the protein within the nanopore is increased to encompass the entire nanopore

<sup>a)</sup>Also at Department of Chemistry and Chemical Biology Rutgers University, 610 Taylor Road, Piscataway, New Jersey 08854, USA.

<sup>b)</sup>Electronic mail: talagad@montclair.edu. URL: <http://www.talaga.name>.

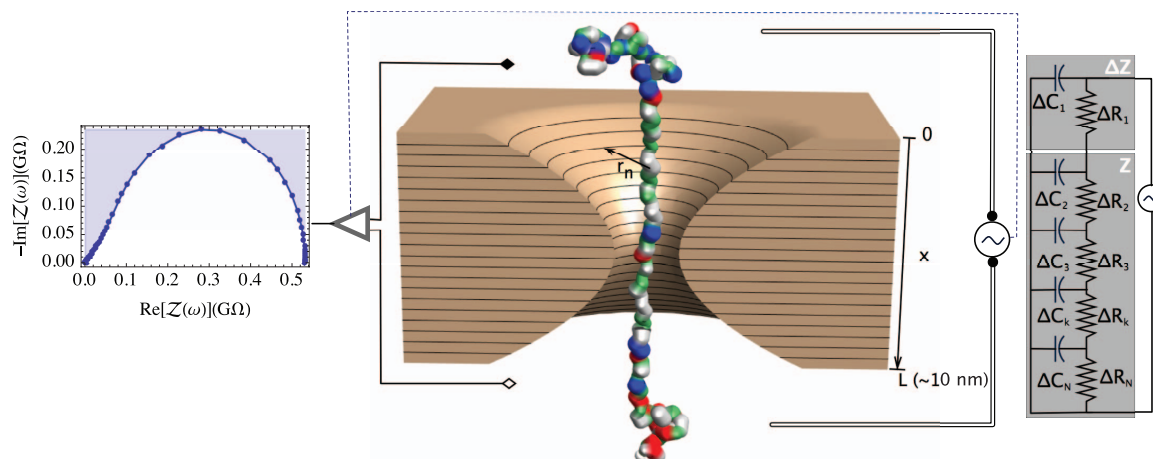


FIG. 1. Experimental schematic for a nanopore EIS experiment on a single unfolded protein molecule. The nanopore contains an electrolyte (not shown). An electrostatically elongated protein traverses a nanopore fitted with electrodes that apply a swept-frequency AC potential (double lines at right) and measure the phase and amplitude of EIS current (single lines at left). Each colored sphere on the protein is an amino acid (red = acidic, blue = basic, green = hydrophilic, gray = hydrophobic.) As the protein passes through the nanopore the groupings of amino acids will be sampled. The amount of excluded volume and surface charge density within each grouping will affect the overall impedance. Geometric variables used in the model are shown in the diagram:  $L$  = length of nanopore,  $r_n(x)$  = radius of nanopore,  $x$  = variable position along axis of pore. The geometric and sequence related variables are mapped into a ladder differential equation<sup>1</sup> describing the equivalent circuit displayed at right.

the EIS spectrum approaches that of an ideal capacitor. When the radius of the protein is set to zero the model should reduce to the original VTW model.

The model connecting protein properties to EIS spectra requires relating amino acid and nanopore surface charge densities to specific differential capacitances. The most common way that protein surface electrical properties are experimentally measured is through the  $\zeta$ -potential, which is interpreted as being the electrostatic potential evaluated at a distance,  $r_\zeta$ , from the protein corresponding to the hydrodynamic slip surface. Therefore, this paper also presents a new approach to relate the  $\zeta$ -potential to the protein double layer specific differential capacitance. The Poisson-Boltzmann equation was numerically solved by a second-order difference method to obtain the double layer potential as a function of distance and surface charge density, which was then expressed in terms of the  $\zeta$ -potential<sup>18–21</sup> enabling a nanopore EIS approach to single molecule or even local chain measurements of the  $\zeta$ -potential.

## II. RESULTS AND DISCUSSION

### A. $Z_{VTW}$ impedance model for a nanopore occupied by a protein

Theoretical treatment of the nanopore without protein began with a differential equation whose solution was previously used to model the influence on EIS of the geometry and double layer specific differential capacitance of nanopores.<sup>1</sup> The diagram at the right of Figure 1 shows a network of infinitesimal capacitive and resistive elements linked in a network to describe just the contribution of nanopore to the impedance. The resistors account for the position dependence of the ionic conductivity through the pore while the capacitors account for the influence of the double layer at the pore walls. One pair of the infinitesimal capacitors and resistors is split off ( $\Delta Z$ ) of the whole circuit ( $Z$ ) to facilitate solution

of the network as a ladder differential equation. Expressing the combination of elements according to the circuit rules and taking the limit as the number of elements goes to infinity and the size of the elements goes to zero, leads to the following differential equation:

$$Z' + i\omega C' Z^2 - R' = 0, \quad (1)$$

where

$$R' = \frac{dR}{dx} = \frac{1}{\pi r_n^2(x)\kappa_n} \quad \text{and} \quad C' = \frac{dC}{dx} = C'(x) = 2\pi r_n(x)\tilde{C}_n. \quad (2)$$

Here  $i = \sqrt{-1}$ ,  $\omega$  is the angular frequency of the AC voltage,  $x$  is the coordinate along the length of the nanopore.<sup>22</sup> The differential impedance ( $Z$ ) includes contributions from the differential capacitance ( $C'$ ) and resistance ( $R'$ ) that depend parametrically on the nanopore radius  $r_n(x)$ .  $\tilde{C}_n$  is the double-layer specific differential capacitance of the solution-nanopore wall interface, and  $\kappa_n$  is the solution conductivity inside the nanopore, which is typically found to be higher than that of the bulk,  $\kappa$ .<sup>23–27</sup> Swapping the order of the resistive and capacitive infinitesimal elements gives the same result: Eq. (1). In this formulation, a nanopore of length zero should have zero impedance, providing the boundary condition,  $Z(0) = 0$ . Additional circuit elements to account for the rest of the apparatus will be introduced below.

For a constant radius,  $r_n(x) = r_n$ , the solution to Eq. (1) is<sup>22</sup>

$$Z_{\text{cyl}}(\omega) = R_{\text{cyl}} \frac{\tanh[\sqrt{i\omega\tau_{\text{cyl}}}]}{\sqrt{i\omega\tau_{\text{cyl}}}}, \quad (3)$$

with

$$R_{\text{cyl}} = \frac{L}{\pi r_n^2 \kappa_n}, \quad (4a)$$

$$\tau_{\text{cyl}} = R_{\text{cyl}} C_{\text{cyl}} = \frac{2L^2 \tilde{C}_n}{r_n \kappa_n}. \quad (4b)$$

An equivalent solution for the network solution can be obtained using a continued fraction approach.<sup>22</sup> Solutions for other geometries (cone, hourglass, lozenge, etc.) are readily obtained from Eq. (1) after replacing  $r(x)$  with the appropriate piecewise linear or quadratic function.<sup>1</sup>

The strong electric fields inside nanopores can unfold and elongate proteins.<sup>11</sup> Consider an elongated and unfolded protein that is traversing the nanopore; the nanopore electrical response will be dominated by the influence of the only portion of the protein within the electrically biased region of the nanopore. To calculate the impedance of the nanopore-protein system, take the protein segment of length  $L$  inside the pore to have effective radius  $r_p$  and a uniform effective surface charge density. The presence of the protein increases the real part of the nanopore impedance by reducing the volume of electrolyte solution in the nanopore. Consider two coaxial cylinders, with the protein being the inner cylinder with radius  $r_p$  and the nanopore being the nanopore with radius  $r_n$  then the cross sectional area available for fluid flow between them is  $\pi(r_n^2(x) - r_p^2(x))$ . The surface charge density on the protein adds a specific differential capacitance to the system, with the total capacitance due to the protein being  $2\pi r_p(x)\tilde{C}_p(x)L$ . Taking the specific differential capacitance on the surface of the protein to be additive with that of the nanopore, Eq. (2) becomes

$$\begin{aligned} R' &= \frac{dR}{dx} = \frac{1}{\pi(r_n^2(x) - r_p^2(x))\kappa_n} \quad \text{and} \\ C' &= \frac{dC}{dx} = 2\pi(r_n(x)\tilde{C}_n + r_p(x)\tilde{C}_p(x)). \end{aligned} \quad (5)$$

The capacitors are additive since parallel capacitors are additive and since the double layers on the surface of the protein and on the surface of the nanopore are in parallel. This however, is not true in the low concentration limit where the double layers on the surface of the protein and on the surface on the nanopore overlap. This occurs when the Debye lengths become comparable to the space between the protein and nanopore.<sup>28,29</sup> In nanopore experiments the electrolyte is not at the low concentration limit.

For constant effective radii,  $r_n(x) = r_n$ ,  $r_p(x) = r_p$  and constant protein double-layer specific differential capacitance,  $\tilde{C}_p(x) = \tilde{C}_p$  the solution to Eq. (1) with the definitions in Eq. (5) for the impedance of a cylindrical nanopore containing a protein becomes

$$Z_{\text{cyl+p}}(\omega) = R_{\text{cyl+p}} \frac{\tanh[\sqrt{i\omega\tau_{\text{cyl+p}}}]}{\sqrt{i\omega\tau_{\text{cyl+p}}}} \quad (6)$$

with

$$R_{\text{cyl+p}} = \frac{L}{\pi(r_n^2 - r_p^2)\kappa_n}, \quad (7a)$$

$$\tau_{\text{cyl+p}} = R_{\text{cyl+p}} C_{\text{cyl+p}} = \frac{2L^2(\tilde{C}_n r_n + \tilde{C}_p r_p)}{(r_n^2 - r_p^2)\kappa_n}. \quad (7b)$$

In Eq. (5) the protein double layer specific differential capacitance  $\tilde{C}_p$  is independent of  $x$ . Each amino acid residue will, however, have a different surface charge density and thus produce a different specific differential capacitance. Thus, the

specific differential capacitance shown here is the effective average of all the residues inside the nanopore. By allowing  $\tilde{C}_p$  to vary with  $x$  one may solve the equation piecewise enabling one to obtain the variation of EIS with protein sequence.  $\tilde{C}_n$  is taken to be independent of  $x$  since nanopores fabricated from homogeneous solid state materials should have a uniform surface charge density.

## B. Limiting behavior of the new model

Equations (7a) and (7b) reduce to Eqs. (4a) and (4b) when the radius of the protein,  $r_p$ , is zero; i.e., there is no protein in the nanopore. Equation (6) reduces to the proper low frequency limit, that of an ideal coaxial electrolyte resistor,

$$\lim_{\omega \rightarrow 0} Z_{\text{cyl+p}}(\omega) = \frac{L}{\pi\kappa_n(r_n^2 - r_p^2)} = R_{\text{cyl+p}}, \quad (8)$$

see, also, Eq. (7a). The high frequency limit of Eq. (6) and its derivative are both zero:

$$\lim_{\omega \rightarrow \infty} Z_{\text{cyl+p}}(\omega) = 0, \quad \lim_{\omega \rightarrow \infty} Z'_{\text{cyl+p}}(\omega) = 0. \quad (9)$$

The peak frequency is found by maximizing  $-\text{Im}[Z_{\text{cyl+p}}(\omega)]$  from Eq. (6) giving

$$\omega_{\text{peak}} \approx 2.54065/\tau_{\text{cyl+p}}. \quad (10)$$

## C. Incorporating the influence of the substrate

The nanopore is fabricated within a substrate, often silicon nitride, its capacitance is given by

$$C_s = \epsilon_s \epsilon_0 A_s / L, \quad (11)$$

where  $\epsilon_0$  is the permittivity of free space,  $\epsilon_s$  is the dielectric constant of the substrate,  $A_s = \pi(r_s^2 - r_n^2)$  is the cross-sectional area of the cylindrical substrate, with  $r_s$  being the substrate's radius, and  $L$  is the thickness of the substrate and the length of the nanopore through the substrate.<sup>2,3,30</sup> The impedance of this substrate, assuming an ideal capacitor, is given by

$$Z_s = \frac{1}{i\omega C_s}. \quad (12)$$

Since the substrate and nanopore are in parallel, the system impedance is the parallel circuit addition of Eqs. (6) and (12):

$$Z_{\text{sys}} = Z_{\text{cyl+p}} \parallel Z_s. \quad (13)$$

A final circuit element could be added to the model to account for the dielectric capacitance of the protein. However, such an element has negligible affect on the EIS spectrum.

Figure 2 shows a Nyquist plot of Eq. (13) for several protein radii and a fixed nanopore radius. The protein sizes were chosen to correspond to polyglycine, polyleucine, and polytryptophan. As the protein radius approaches that of the nanopore, the EIS spectrum approaches that of an ideal capacitor, as expected. The system contains a tubular protein within a hole in a substrate. As the tube fills the hole, the substrate becomes blocked, and thus is simply a flat substrate, which would behave as a capacitor.

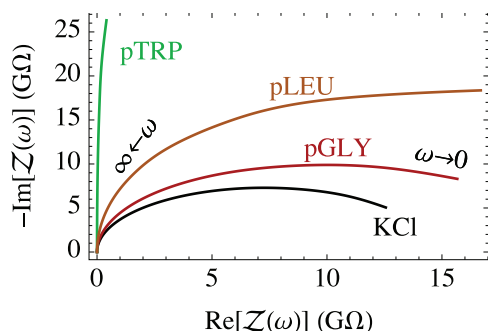


FIG. 2. The effect on EIS spectra of varying protein radius,  $r_p$  using Eq. (13) with  $L = 9.5$  nm,  $r_n = 0.438$  nm,  $r_s = 50$   $\mu$ m,  $\kappa = 1.09$  S/m (100 mM KCl),  $\tilde{C}_n = 1$  mF/m<sup>2</sup>,  $\tilde{C}_p = 10$  mF/m<sup>2</sup>, and  $\epsilon_s = 6$ . The black, red, orange, and green lines correspond to the protein-free pore ( $r_p = 0$  nm), polyglycine ( $r_p = 0.224$  nm), poly-leucine ( $r_p = 0.375$  nm), and poly-tryptophan ( $r_p = 0.437$  nm), respectively. In the limit that the radius of the protein is equal to that of the nanopore, the response becomes that of an ideal capacitor.

Figure 3 shows the negative imaginary impedance from Eq. (13) vs. frequency for several different values of the protein specific differential capacitance. As the protein is traversing the nanopore, different regions on the protein will have varying amounts of surface charge density. This surface charge density produces the double-layer specific differential capacitance when the protein is in a conducting solution. The value of this capacitance can be obtained from the time constant (Eq. (7b)) in Eq. (13).

Equations (7a) and (7b) are defined by six physical parameters,  $r_p$ ,  $r_n$ ,  $\tilde{C}_p$ ,  $\tilde{C}_n$ ,  $L$  and  $\kappa_n$ . However, these equations only give two experimentally measurable parameters,  $\tau_{\text{cyl}+p}$  and  $R_{\text{cyl}+p}$ . To obtain all six parameters, first a calibration of the nanopore must be performed to obtain the geometric parameters of the nanopore using Eqs. (4a) and (4b) as previously shown.<sup>1</sup> After the three geometric parameters of the nanopore and the nanopore conductivity are known, then the protein parameters may be obtained.

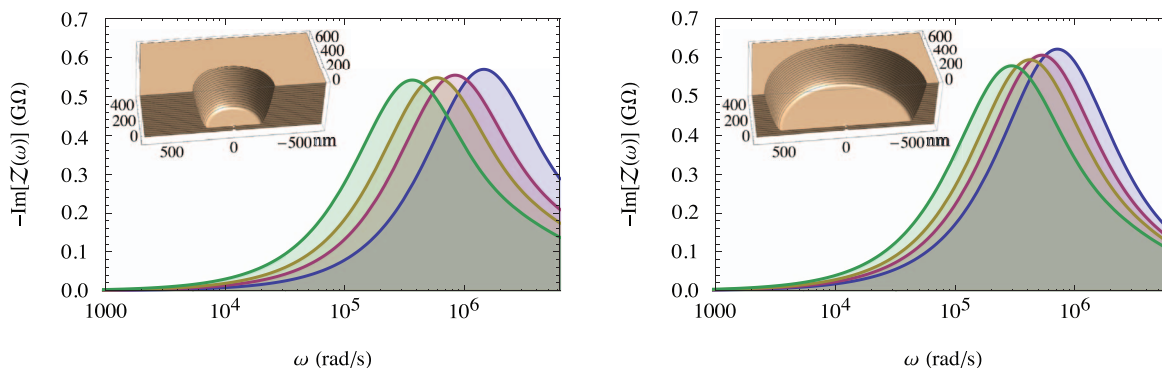


FIG. 3. Effect of membrane structure on EIS resolution of the protein surface charge density. The panels differ only by the radius of the thin membrane containing the nanopore. Left: Membrane radius  $r_s = 200$  nm. Right:  $r_s = 500$  nm. The insets show schematically the changes in the membrane holding the nanopore. The peak angular frequency moves to lower values with lower values of  $\tilde{C}_p$ . The additional capacitance of the larger area of the membrane holding the nanopore compresses the differences in the characteristic response time that arise due to the changes in polypeptide surface charge. The negative imaginary component of Eq. (13) was plotted with  $L = 60$  nm,  $r_n = 4$  nm,  $r_p = 1.5$  nm, the experimentally determined<sup>1</sup> nanopore double layer specific differential capacitance  $\tilde{C}_n = 1$  mF/m<sup>2</sup>, the numerically calculated protein double layer specific differential capacitance  $\tilde{C}_p = 2.0, 3.8, 5.6, 9.2$  F/m<sup>2</sup>, blue, red, yellow, green, respectively, with  $\sigma = 0.1, 0.2, 0.3,$  and  $0.5$  C/m<sup>2</sup> and the corresponding  $\zeta$ -potentials of 29, 38, 41, and 44 mV. The  $\zeta$ -potential was calculated by numerically solving Eq. (16) and evaluating at the slip plane, with  $\epsilon_s = 6$  (silicon nitride),  $T = 297$  K, and  $\kappa = 1.09$  S/m (100 mM KCl),  $\epsilon_s = 80$ . The slip plane was taken to be  $r_\zeta = 0.7$  nm from the protein, or size of one hydrated counter-ion.  $\tilde{C}_p$  was calculated from Eq. (23) by numerically solving Eq. (16) evaluating the potential at the protein surface, then numerically differentiating with respect to the surface charge density.

Figure 3 also illustrates the influence of the substrate response on the resolution of EIS with respect to the charge on the protein. The response of the substrate is dominated by the capacitance of the thin membrane surrounding the nanopore. The left panel shows a substrate geometry consistent with a thin nanopore sculpted from a larger nanopore drilled through a thick substrate (i.e., focussed ion beam drilling followed by noble gas ion sculpting<sup>2,3</sup>). The right panel shows the EIS resolution of different surface charges by nanopore drilled through a thin substrate (i.e., TEM drilling<sup>30</sup>). The nanopore is identical in both. The difference is that the thin portion of the substrate where the nanopore is located has a larger surface area in the right panel case than in the left panel case. The additional capacitance of the larger area of the membrane holding the nanopore compresses the differences in the characteristic response time that arise due to the changes in polypeptide surface charge. This result suggests that the geometry of the substrate surrounding the nanopore may significantly influence the sensitivity and resolution of EIS-based nanopore experiments. In particular the nanopore geometry resulting from focussed ion beam drilling through thicker substrate windows followed by noble gas ion beam sculpting to obtain the nanopores may have significant advantages over TEM drilling as currently implemented. The surface area of the thin membrane containing the nanopore must be minimized while still maintaining sufficiently low resistance so as to not contribute significantly to the transient impedance drop across the device.

#### D. $\zeta$ -potential and numerical solutions to the specific differential capacitance

In this section an expression for the  $\zeta$ -potential<sup>18–21</sup> and double layer specific differential capacitance for a long tube is developed. Both the double layer specific differential capacitance of a protein and its  $\zeta$ -potential arise from the surface charge density and depend on the solution conditions through

the pH dependence of the protein ionization state and through the double-layer dependence on the electrolyte concentration via the Debye length,

$$\lambda_D = \left( \frac{\epsilon_r \epsilon_0 k_B T}{\sum_{i=1}^N n_i^0 q_i^2} \right)^{1/2}. \quad (14)$$

Since both  $\tilde{C}_p$  and the  $\zeta$ -potential are related to the surface charge density, determination of any one of the three quantities allows the other two to be determined. Since the  $\zeta$ -potential is a routinely measured quantity it would be invaluable to have an expression to calculate the double-layer specific differential capacitance or surface charge density from the  $\zeta$ -potential. EIS is sensitive to the local specific differential capacitance, thus enabling, in principle, a method to measure the *local*  $\zeta$ -potential values of a long heterogeneous polymer.

Beginning with Poisson-Boltzmann equation<sup>13,31</sup> for a long cylinder, where the potential is independent of the length and angular coordinate,

$$\frac{1}{r} \frac{d}{dr} r \frac{d\Phi(r)}{dr} = -\frac{q}{\epsilon_0 \epsilon_r} \sum_i n_i^0 z_i \exp \left[ \frac{-z_i q \Phi(r)}{k_B T} \right], \quad (15)$$

where  $\Phi$  is the potential,  $k_B$  is Boltzmann's constant,  $T$  is absolute temperature,  $q$  is the elementary charge,  $z$  is the valency,  $n_i$  is the species density in the lamina, and  $n_i^0$  is the bulk species density infinitely far from the potential source. Consider simplifying this for a 1:1 electrolyte such as KCl, where  $n_1^0 = n_2^0 = n^0$ ,  $z_1 = 1$ , and  $z_2 = -1$ :

$$\frac{1}{r} \frac{d}{dr} r \frac{d\Phi(r)}{dr} = \frac{2qn^0}{\epsilon_0 \epsilon_r} \sinh \left[ \frac{q\Phi(r)}{k_B T} \right]. \quad (16)$$

For potentials such that  $q\Phi$  is less than  $k_B T$ , around 20 mV, one can linearize Eq. (16) by retaining the first term of the series expansion of sinh:

$$\frac{1}{r} \frac{d}{dr} r \frac{d\Phi(r)}{dr} = \frac{2q^2 n^0}{\epsilon_0 \epsilon_r k_B T} \Phi(r) = \lambda_D^{-2} \Phi(r), \quad (17)$$

where  $\lambda_D$  is the Debye length. With the standard boundary conditions:

$$\lim_{r \rightarrow \infty} \Phi(r) = 0, \quad (18)$$

that is, as the distance from the surface is large the potential approaches zero. Also,

$$\sigma = -\epsilon_r \epsilon_0 \left( \frac{d\Phi}{dr} \right)_{r=r_p}, \quad (19)$$

where  $\sigma$  is the surface charge density, and  $r_p$  is the tube radius of the protein, which yields

$$\Phi(r) = \frac{\sigma \lambda_D K[0, r/\lambda_D]}{\epsilon_r \epsilon_0 K[1, r_p/\lambda_D]} \quad r \geq r_p, \quad (20)$$

where  $K$  is the modified Bessel function of the second kind. The  $\zeta$ -potential can be found by evaluating  $\Phi(r)$  at the slip plane, that is at  $r = r_p + r_\zeta$ :

$$\zeta = \frac{\sigma \lambda_D K[0, (r_p + r_\zeta)/\lambda_D]}{\epsilon_r \epsilon_0 K[1, r_p/\lambda_D]}, \quad (21)$$

where  $r_\zeta$  is the distance from the surface of the tube to the slip plane. Using a measured  $\zeta$ -potential and inverting the above equation, one can calculate the net surface charge density on the tube or protein,

$$\sigma = \frac{\zeta \epsilon_r \epsilon_0 K[1, r_p/\lambda_D]}{\lambda_D K[0, (r_p + r_\zeta)/\lambda_D]}. \quad (22)$$

Each amino acid residue will contribute a given amount of surface charge density; the net surface charge density being the weighted sum of the contribution from each residue, weighted by the surface area of the residue.

Next consider the specific differential capacitance due to the electrical double layer on the surface of the tube. The specific differential capacitance is related to the surface charge density by

$$\tilde{C} = \frac{d\sigma}{d\Phi_0}, \quad (23)$$

where  $\Phi_0 = \Phi(r_p)$  is the potential at the surface of the protein.<sup>32</sup> Solving Eq. (20) for the surface charge density, while evaluating this at the radius of the protein

$$\sigma = \frac{\Phi_0 \epsilon_r \epsilon_0 / \lambda_D K[1, r_p]}{\lambda_D K[0, r_p/\lambda_D]}, \quad (24)$$

then differentiating with respect to the surface potential yields the electrical double-layer specific differential capacitance:

$$\tilde{C} = \frac{\epsilon_r \epsilon_0 K[1, r_p/\lambda_D]}{\lambda_D K[0, r_p/\lambda_D]}. \quad (25)$$

Equation (25) represents the linearized case and is independent of the surface potential. To obtain a surface charge density dependent specific differential capacitance, Eq. (16) was solved numerically by a second-order finite difference method<sup>33</sup> as a function of  $\sigma$  and  $r_p$ . Direct substitution verified convergence and showed an error of less than 1 ppm. The resulting potential was numerically differentiated with respect to  $\sigma$  at  $r_p$  to obtain the specific differential capacitance through Eq. (23):

$$\frac{1}{\tilde{C}} \approx \frac{\Phi_0(\sigma + \Delta\sigma) - \Phi_0(\sigma - \Delta\sigma)}{2\Delta\sigma}. \quad (26)$$

## E. Transient analysis

The sensitivity to charge and volume sequence differences, as illustrated in Figs. 2 and 3, suggested that coarse-grain sequence information may be accessible from EIS measurements made in such a way as to probe local segments of the polypeptide chain. It was assumed that the position of the protein is static at each instance of measurement, and that the applied AC field is weak resulting in no nanopore electric field enhancement of ionization ( $\Delta pK_a = 0$ ). Volume in the pore was determined by summing the amino acid residue

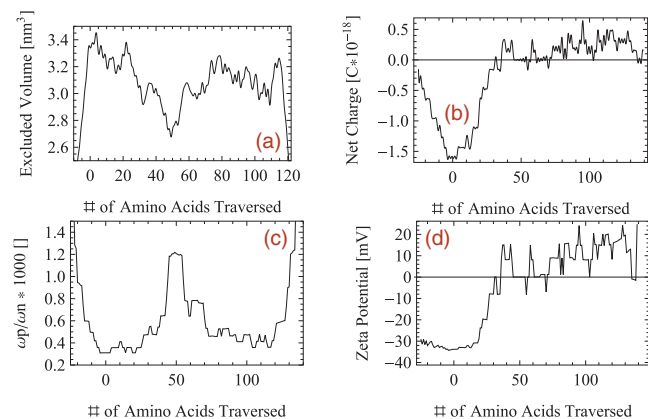


FIG. 4. Dependence of EIS parameters and local  $\zeta$ -potential on the local protein volume and charge as a function of amino acids traversed during unfolded linear human  $\alpha$ Syn translocation starting with the C-terminus. The translocation coordinate corresponds to the number of amino acids that have passed completely through the  $L = 9.5$  nm nanopore (25 amino acids inside). Panel (a) shows the excluded volume; panel (b) shows the net charge on the amino acids present in the nanopore. The fluctuations in local excluded volume and net charge arise because of the different amino acids at different locations in the sequence. Panel (c) shows the changes in peak EIS frequency during translocation. The ends of the translocation coordinate show that the peak increases to that of the protein-free nanopore. The peak in the middle corresponds to the NAC region of  $\alpha$ Syn, which has relatively little charge. Panel (d) shows the local protein  $\zeta$ -potential as a function of number of amino acids traversed calculated from Eq. (21) using  $r_n = 4$  nm,  $\tilde{C}_n = 1$  mF/m<sup>2</sup>,  $T = 297$  K,  $\kappa = 1.09$  S/m (100 mM KCl),  $\epsilon_s = 80$ , and  $r_c = 0.7$  nm ( $\sim$  the diameter of one hydrated counter-ion).

volumes,<sup>11,34</sup> and using pKa data<sup>35</sup> in Eq. (27):

$$Q_{\text{prot}} = \sum_{j=\xi}^{n+\xi} \pm (10^{\pm(\text{pH}-\text{pKa}_j-\Delta\text{pKa}_j)} + 1)^{-1}. \quad (27)$$

The translocation coordinate is defined as the number of amino acids that have passed entirely through the nanopore. The average value of the length of an amino acid in an extended  $\beta$ -strand structure is about 0.38 nm. Therefore, a nanopore of length  $L = 9.5$  nm will contain approximately 25 amino acids. Once inside the nanopore, the protein segment EIS response depends on the surface charge density and size of the amino acids in the nanopore and not on their relative positions in the nanopore.

Panels (a) and (b) in Fig. 4 show the excluded volume and the absolute value of the charge of human  $\alpha$ Syn in the nanopore as a function of number of amino acids that have traversed the nanopore starting from the C-terminus. The relative magnitude of the fluctuations increases for shorter nanopores due to there being fewer amino acids present inside it. Panel (c) in Fig. 4 shows the peak frequency of the EIS curve as a function of number of amino acids that have traversed the nanopore. Notice at the end points of the translocation, the peak frequency appears to diverge. This feature shows the entrance and exit of the protein from the nanopore and the return of the peak frequency to the empty nanopore value. With no protein in the nanopore the time constant is small yielding a large peak frequency. As the double-layer specific differential capacitance in the nanopore from the protein increases the time constant also increases, thus decreasing the peak frequency. The peak frequency rises again near the center of

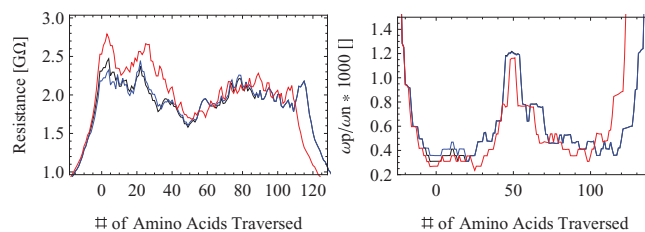


FIG. 5. Sequence effects on EIS. Human  $\alpha$ Syn and  $\beta$ Syn are shown in black and red, respectively, while mouse  $\alpha$ Syn is shown in blue. The left panel shows a comparison of the resistances as a function of number of amino acids traversed as calculated using Eq. (7a), with  $L = 9.5$  nm,  $r_n = 2.0$  nm, and  $r_p$  as in Fig. 4. The right panel shows the peak frequencies as a function of number of amino acids traversed calculated as in Fig. 4(c) for each of the synuclein variants.

Fig. 4(c) due to the lack of surface charge density in the central region of human  $\alpha$ Syn. The protein double layer specific differential capacitance was calculated by numerically solving Eq. (16) and evaluating the solution at the surface of the protein, then using Eq. (26) while assuming that the amino acid charge was distributed across its surface area. Amino acid surface areas were taken from Samanta *et al.*<sup>36</sup> It was also assumed that the specific differential capacitance from each amino acid is additive. Deviations from this assumption may arise from mixing of the solution near the boundary of each amino acid. This value of the specific differential capacitance was used to calculate the characteristic time constant of the system (Eq. (7b)) and converted to the peak frequency (Eq. (10)). The time constant of the system with the protein in the nanopore (Eq. (7b)) is also a function of the radius of the protein. The radii were calculated by assuming a cylindrical volume with the average length of each amino acid. Then the average value of the radii of the amino acids in the nanopore at a given time was used. Figure 4(d) shows the predicted dependence of the local  $\zeta$ -potential of the protein segment inside the nanopore on translocation position calculated by numerically solving Eq. (16) and evaluating the results at the slip plane. Notice the linearized zeta potential, Eq. (21), is linearly proportional to the surface charge density. Thus, using Eq. (21) would lead only to a scaling of the surface charge density.

Figure 5 illustrates changes predicted in EIS for three closely related proteins: human  $\alpha$ Syn, mouse  $\alpha$ Syn, and human  $\beta$ Syn.<sup>22</sup> There are seven point mutations between human  $\alpha$ Syn and mouse  $\alpha$ Syn: A53T, S87N, L100M, N103G, A107Y, D121G, and N122S. Most of the differences appear in the C-terminal region, which should thread first into the nanopore, inducing changes between 0 and 20 in the nanopore translocation coordinate. These relatively small sequence differences show up in Fig. 5(a) as  $\sim 5\%$  changes in resistance and in Fig. 5(b) as  $\sim 5\%$  changes in peak frequency. Human  $\beta$ Syn has many deletions and only a 67% sequence homology with  $\alpha$ Syn had showed substantially larger changes in resistance and peak frequency, though the differences are again concentrated in the C-terminal region, consistent with the sequence.

### III. CONCLUSION

A model that was successfully used to model the influence of nanochannel shape and surface charge properties on

impedance spectra was extended to include the influence of an unfolded protein also being present. The extended model predicts the impedance of a protein traversing a nanopore, where the protein has been simplified to a tube of varying diameter and surface charge. The model provided physically correct limiting behavior; in the absence of the protein, the model reduces to the original VTW impedance model. Exploration of the theory suggested that EIS may be used to distinguish the size and surface charge on the protein that is present in the nanopore during translocation. The model is able to distinguish one charged region from another on a protein or similar structure through the effect on the peak frequency in the negative imaginary impedance. The model shows that the surface area of the thin membrane containing the nanochannel contributes a capacitance that reduces the resolution of the proposed EIS experiments. The VTW geometric model formalism provides a design principle for designing nanochannel devices for protein identification. Illustrative calculations show how even fairly closely related proteins may be distinguishable using EIS.

## ACKNOWLEDGMENTS

This project was supported in part by the National Institute of General Medical Sciences under Award No. R01GM071684. The authors thank the National Science Foundation for partial support of this work through a NIRT Grant No. 0609000. The content is solely the responsibility of the authors and does not necessarily represent the official views of the National Institute of General Medical Sciences, the National Institutes of Health, or the National Science Foundation.

## NOMENCLATURE

|                       |   |                       |
|-----------------------|---|-----------------------|
| $Z$                   | Impedance   | [ $\Omega$ ]          |
| $R$                   | Resistance  | [ $\Omega$ ]          |
| $C$                   | Capacitance   | [F]                   |
| $Z'$                  | Differential impedance                                  | [ $\Omega/\text{m}$ ] |
| $R'$                  | Differential resistance                                 | [ $\Omega/\text{m}$ ] |
| $C'$                  | Differential capacitance                                | [F/m]                 |
| $\omega$              | Angular frequency                                       | [rad/s]               |
| $i$                   | $\sqrt{-1}$   | [...]                 |
| $r$                   | Radius  | [m]                   |
| $\tilde{C}_n$         | Nanopore double-layer specific differential capacitance | [F/m <sup>2</sup> ]   |
| $\tilde{C}_p$         | Protein double-layer specific differential capacitance  | [F/m <sup>2</sup> ]   |
| $\kappa_n$            | Nanopore conductivity                                   | [S/m]                 |
| $L$                   | Nanopore length   | [m]                   |
| $Z_{\text{cyl}}$      | Cylindrical impedance model                             | [ $\Omega$ ]          |
| $R_{\text{cyl}}$      | Resistance of a cylinder                                | [ $\Omega$ ]          |
| $r_n$                 | Nanopore radius   | [m]                   |
| $r_p$                 | Protein radius  | [m]                   |
| $r_s$                 | Substrate radius  | [m]                   |
| $\tau_{\text{cyl}}$   | Time constant for constant radius nanopore              | [s]                   |
| $Z_{\text{cyl+p}}$    | Cylindrical plus protein impedance model                | [ $\Omega$ ]          |
| $R_{\text{cyl+p}}$    | Resistance of a cylinder plus protein                   | [ $\Omega$ ]          |
| $C_{\text{cyl+p}}$    | Nanopore and protein double layer capacitance           | [F]                   |
| $\tau_{\text{cyl+p}}$ | Time constant for constant radius nanopore plus protein | [s]                   |
| $C_s$                 | Substrate capacitance                                   | [F]                   |
| $A_s$                 | Substrate area  | [m <sup>2</sup> ]     |

|                  |   |                     |
|------------------|---|---------------------|
| $Z_s$            | Substrate impedance                         | [ $\Omega$ ]        |
| $Z_{\text{sys}}$ | System impedance                            | [ $\Omega$ ]        |
| $\epsilon_0$     | Permittivity of free space                  | [F/m]               |
| $\epsilon_s$     | Substrate dielectric constant               | [...]               |
| $\Phi$           | Potential                                   | [J/C]               |
| $q$              | Elementary charge                           | [C]                 |
| $k_B$            | Boltzmann constant                          | [J/K]               |
| $T$              | Temperature                                 | [K]                 |
| $n_i$            | Species density in lamina                   | [1/m <sup>3</sup> ] |
| $n_i^0$          | Bulk species density                        | [1/m <sup>3</sup> ] |
| $z$              | Valency                                     | [...]               |
| $\lambda_D$      | Debye length                                | [m]                 |
| $K$              | Modified Bessel function of the second kind | [...]               |
| $\sigma$         | Surface charge density                      | [C/m <sup>2</sup> ] |
| $\Phi_0$         | Surface potential                           | [J/C]               |
| $\zeta$          | $\zeta$ -Potential                          | [J/C]               |

- M. J. Vitarelli, S. Prakash, and D. S. Talaga, *Anal. Chem.* **83**, 533 (2011).
- C. Dekker, *Nat. Nanotechnol.* **2**, 209 (2007).
- A. Piruska, M. Gong, J. V. Sweedler, and P. W. Bohn, *Chem. Soc. Rev.* **39**, 1060 (2010).
- Y. Tian, X. Hou, L. Wen, W. Guo, Y. Song, H. Sun, Y. Wang, L. Jiang, and D. Zhu, *Chem. Commun.* **46**, 1682 (2010).
- Z. Siwy and S. Howorka, *Chem. Soc. Rev.* **39**, 1115 (2010).
- J. K. Holt, H. G. Park, Y. Wang, M. Stadermann, A. B. Artyukhin, C. P. Grigoropoulos, A. Noy, and O. Bakajin, *Science* **312**, 1034 (2006).
- Z. Siwy, E. Heins, C. Harrell, P. Kohli, and C. Martin, *J. Am. Chem. Soc.* **126**, 10850 (2004).
- E. Steinle, D. Mitchell, M. Wirtz, S. Lee, C. Young, and V. Y. Martin, *Anal. Chem.* **74**, 2416 (2002).
- S. Howorka and Z. Siwy, *Chem. Soc. Rev.* **38**, 2360 (2009).
- Z. Chen, Y. Jiang, D. R. Dunphy, D. P. Adams, C. Hodges, N. Liu, N. Zhang, G. Xomeritakis, X. Jin, N. R. Aluru, S. J. Gaik, H. W. Hillhouse, and C. J. Brinker, *Nature Mater.* **9**, 667 (2010).
- D. Talaga and J. Li, *J. Am. Chem. Soc.* **131**, 9287 (2009).
- D. Branton, D. W. Deamer, A. Marziali, H. Bayley, S. A. Benner, T. Butler, M. Di Ventra, S. Garaj, A. Hibbs, X. Huang, S. B. Jovanovich, P. S. Krstic, S. Lindsay, X. S. Ling, C. H. Mastrangelo, A. Meller, J. S. Oliver, Y. V. Pershin, J. M. Ramsey, R. Riehn, G. V. Soni, V. Tabard-Cossa, M. Wanunu, M. Wiggin, and J. A. Schloss, *Nat. Biotechnol.* **26**, 1146 (2008).
- A. J. Bard and L. R. Faulkner, *Electrochemical Methods: Fundamentals and Applications* (John Wiley and Sons, 1980).
- E. Barsoukov, and R. MacDonald, in *Impedance Spectroscopy: Theory, Experiment, and Applications*, 2nd ed., edited by E. Barsoukov, and R. MacDonald (Wiley-Interscience, 2005), p. 608.
- J. R. Macdonald, in *Impedance Spectroscopy: Emphasizing Solid Materials and Systems*, edited by J. R. Macdonald (John Wiley and Sons, 1987).
- E. N. Ervin, H. S. White, L. A. Baker, and C. R. Martin, *Anal. Chem.* **78**, 6535 (2006).
- E. N. Ervin, H. S. White, and L. A. Baker, *Anal. Chem.* **77**, 5564 (2005).
- N. Amani, M. Saberi, and J. Chamani, *Protein Pept. Lett.* **18**, 935 (2011).
- A. Doostmohammadi, A. Monshi, R. Salehi, M. Fathi, Z. Golniya, and A. Daniels, *Ceram. Int.* **37**, 2311 (2011).
- P. Leroy, C. Tournassat, and M. Bizi, *J. Colloid Interface Sci.* **356**, 442 (2011).
- Z. Omidvar, K. Parivar, H. Sane, Z. Amiri-Tehranizadeh, A. Baratian, M. Saveri, A. Asoodeh, and J. Chamani, *J. Biomol. Struct. Dyn.* **29**, 181 (2011).
- See supplementary material at <http://dx.doi.org/10.1063/1.4819470> for a derivation of Eq. (1); for details of the solution of Eq. (1) for constant radius (cylindrical pore); for a recursion formula approach to solving the network equivalent circuit that gives the same results as Eq. (1); and for aligned sequences for the three synuclein proteins.
- C. Desgranges and J. Delhommelle, *Phys. Rev. E* **77**, 027701 (2008).
- R. Karnik, R. Fan, M. Yue, D. Li, P. Yang, and A. Majumdar, *Nano Lett.* **5**, 943 (2005).
- R. B. Schoch, H. van Lintel, and P. Renaud, *Phys. Fluids* **17**, 100604 (2005).
- D. Stein, M. Kruithof, and C. Dekker, *Phys. Rev. Lett.* **93**, 035901 (2004).
- Y. W. Tang, I. Szalai, and K.-Y. Chan, *Mol. Phys.* **99**, 309 (2001).
- S. Pennathur and J. G. Santiago, *Anal. Chem.* **77**, 6772 (2005).

- <sup>29</sup>S. Pennathur and J. G. Santiago, *Anal. Chem.* **77**, 6782 (2005).
- <sup>30</sup>M. P. Shaurya Prakash and K. Bellman, *J. Micromech. Microeng.* **22**, 067002 (2012).
- <sup>31</sup>J. O. Bockris and A. K. Reddy, *Modern Electrochemistry I: Ionics*, 2nd ed. (Plenum Publishing Corp., 1998).
- <sup>32</sup>A. A. Kornyshev, *J. Phys. Chem. B* **111**, 5545 (2007).
- <sup>33</sup>K. E. Atkinson, *An Introduction to Numerical Analysis* (John Wiley & Sons, Inc., 1989).
- <sup>34</sup>S. Perkins, *Eur. J. Biochem.* **157**, 169 (1986).
- <sup>35</sup>Y. Nozaki and C. Tanford, *Methods Enzymol.* **11**, 715 (1967).
- <sup>36</sup>U. Samanta, R. Bahadur, and P. Charkrabarti, *Protein Eng.* **15**(8), 659 (2002).